International Journal on Magnetic Particle Imaging
Vol 10, No 1, Suppl 1, Article ID 2403023, 4 Pages

Infinite Science Publishing

Proceedings Article

Analysis of noise sources in a human-scale fMPI imager

Frauke H. Niebel [a,b,c*] · Jorge Chacon-Caldera [c,f] · Eli Mattingly [c,d,e] · Alex C. Barksdale [c,e] · Monika Śliwiak [c] · Lawrence L. Wald [c,d,f]

[a] Fraunhofer Research Institution for Individualized and Cell-Based Medical Engineering IMTE, Lübeck, Germany
[b] Institute of Medical Engineering, University of Lübeck, Lübeck, Germany
[c] Martinos Center for Biomedical Imaging, Massachusetts General Hospital, Charlestown, MA, USA
[d] Harvard-MIT Division of Health Sciences & Technology, Cambridge, MA, USA
[e] Massachusetts Institute of Technology, Cambridge, MA, USA
[f] Harvard Medical School, Boston, MA, USA
[*] Corresponding author, email: frauke.niebel@student.uni-luebeck.de

© 2024 Niebel *et al.*; licensee Infinite Science Publishing GmbH

This is an Open Access article distributed under the terms of the Creative Commons Attribution License (http://creativecommons.org/licenses/by/4.0), which permits unrestricted use, distribution, and reproduction in any medium, provided the original work is properly cited.

Abstract

High sensitivity is a key benefit of magnetic particle imaging (MPI) and drives many of its applications, including functional neuroimaging (fMPI). Since the thermal noise levels expected from the preamplifier and coil resistance are quite low, it is crucial to identify, characterize and remove any fluctuations which appear similar to true thermal dissipative noise, including those originating from external interference sources or system instabilities. These include fluctuations in the gain or production of genuine harmonics originating from the SPIONs as well as nuisance fluctuations of empty-bore signals at each harmonic frequency. While stable empty-bore harmonic signals can be calibrated and subtracted from the detected data, uncontrolled variance in their levels appears as "noise" and can ultimately limit the achievable signal-to-noise ratio (SNR) of the scanner. Here, we present a characterization of these noise source mechanisms in our human-scale field-free line (FFL) fMPI scanner. Currently, the shift amplifier, which is responsible for the translation of the FFL across the field of view (FOV), is the dominant source of noise. Eliminating the shift noise and improving the system's stability would improve our sensitivity from our current detection limit of 150 ng to 15 ng of iron, a 10× improvement.

I. Introduction

Sensitivity to small changes in tracer concentration is a primary metric of MPI and other exogenous tracer-based imaging methods. For example, future applications characterizing cerebral hemodynamics such as functional brain mapping, stroke, perfusion, angiographic imaging, etc. will compete with similar hemodynamic contrast mechanisms in MRI and sensitivity will be a primary distinguishing characteristic. In order to maximize MPI's signal-to-noise ratio (SNR), it is vital to identify and characterize any sources of random noise or systematic background signals interfering with detection of the particle signal. Here, we present a characterization of noise and background signal generating mechanisms for our field-free line (FFL)-based fMPI imager for human brain applications [1]. Previous work has presented MPI noise characterization for a commercial MPI scanner (Bruker, Ettlingen, Germany) [2, 3]. Additionally, the issue of unstable background signals related to image reconstruction has been discussed [4]. However, these do not reflect the increased hardware requirements of

10.18416/ijmpi.2024.2403023

© 2024 Infinite Science Publishing

a human-sized system. This work focuses on the four major subsystems of our scanner setup, namely 1) the receive chain including an AD8429 low-noise preamplifier (Analog Devices, Wilmington, MA, USA) and an 1:2 impedance matching transformer, 2) the transmit chain with an AE Techron 8512 (AE Techron, Elkhart, IN, USA) drive amplifier, drive filter and coil, 3) the FFL gantry rotation system employing a 3 HP (2.2 kW) motor and its controller and monitoring system and 4) the shift system to translate the FFL, consisting of an amplifier (IECO MPS 300-700) powering the pair of electromagnets through a rotary slip-ring [5]. To study the contribution from each of these subsystems to the total image noise, we quantify their contributions to the noise of each harmonic. To guide our future optimization efforts, we estimate the SNR improvement factor expected if we succeeded in the elimination of each subsystems' noise contribution.

II. Methods and materials

To assess the contribution of each of the four subsystems to the noise at the harmonics of $f_0 = 26.3\,\mathrm{kHz}$, we acquired empty-bore measurements for which each subsystem was turned on separately. The exact measurement protocol was: 1) All subsystems off, 2) preamplifier on, 3) preamp plus drive amplifier on (3.5 mT drive field amplitude requiring 30 A in the human-head-sized drive coil), 4) preamp plus motor on and 5) preamp plus shift amplifier on (but no current output). Each of the 22.8-ms empty-bore acquisitions was recorded 100 times. For each measurement, we calculated the root-mean-square (RMS) power spectral density ($\sqrt{\mathrm{PSD}}$) and normalized by the receive chain transfer function T_{Rx} to convert the recorded voltage to an estimate of the magnetic moment required to create that voltage level. The standard deviation of this quantity yields the imager's noise floor $S_{\mathrm{Noise}} = \mathrm{std}(\sqrt{\mathrm{PSD}}/T_{\mathrm{Rx}})$ in units of $\mathrm{Am}^2/\sqrt{\mathrm{Hz}}$. To determine the transfer function of the receive chain T_{Rx}, a known magnetic moment (current loop printed on a circuit board) was placed inside the receive coil and its drive frequency was swept from 1kHz to 250kHz. Moreover, we include simulated receive coil noise estimated from an in-house Biot-Savart model (available at https://github.com/EliMattingly22/Biot.jl).

III. Results

Figure 1A shows the contribution from each of the four specified subsystems to the imager's noise floor (S_{Noise}). Receive coil noise is shown as the dashed line. The contributions to the noise at the harmonics are marked by open circles. To visualize the scaling between the noise from different sources, Figure 1B and Figure 1C show the contributions from the upstream noise sources relative to the preamplifier noise and, respectively, the receive coil noise. We report noise values for frequencies up to $9f_0$ and explicitly list the relative values for the noise at $3f_0$ (dark red box in Figure 1).

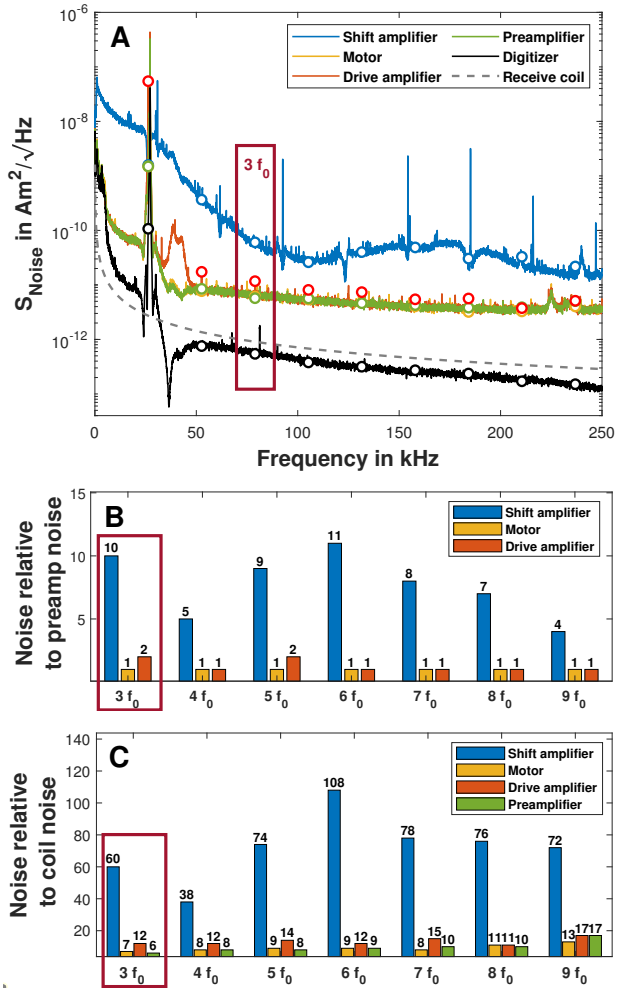

Figure 1: **A** Standard deviation of Spectral density of imager noise (S_{Noise}) for the four interference subsystems. Digital noise is represented by the black line. Receive coil noise is added as a simulated quantity (gray dashed line). The harmonics are marked by open circles.**B** Noise from the shift amplifier, the motor and the transmit chain normalized to preamplifier noise. **C** Noise from all subsystems relative to receive coil noise.

With all subsystems turned off, the baseline noise level ($0.54\,\mathrm{pAm}^2/\sqrt{\mathrm{Hz}}$) is set by digital noise (black line) generated during the quantization process. Turning the preamplifier on (green line) increases the imager's noise level by a factor of 6 ($5.71\,\mathrm{pAm}^2/\sqrt{\mathrm{Hz}}$) relative to receive coil noise ($0.91\,\mathrm{pAm}^2/\sqrt{\mathrm{Hz}}$). The drive current (red line) does not raise the overall noise floor but adds a systematic variance at each harmonic which increases the 3rd harmonic's fluctuations by a factor of 2 compared to preamplifier noise and a factor of 12 compared to coil noise ($11.71\,\mathrm{pAm}^2/\sqrt{\mathrm{Hz}}$). Switching the drive amplifier off and the motor on reverts the noise floor to the level

© 2024 Infinite Science Publishing

of preamplifier noise yielding a comparable value of 6.13 $pAm^2/\sqrt{Hz}$. The shift amplifier (blue line) massively elevates the imager's noise floor (60.43 $pAm^2/\sqrt{Hz}$) resulting in an increase of the noise by a factor of 10 compared to preamplifier noise and a factor of 60 relative to receive coil noise. The peak at the fundamental frequency is likely a divide-by-zero artifact arising from the notch in the receive chain transfer function.

IV. Discussion

Among the investigated subsystems, the shift amplifier is the dominant noise source with a noise floor 10× above the noise level of the preamplifier. If we succeeded in the elimination of the shift noise, the noise at the 3rd harmonic would be reduced by a factor of 5 with the drive turned on. This suggests an SNR improvement by a factor of 5. Moreover, we observed that the shift noise is significantly lower in our smaller non-human primate receive coil suggesting it is coupling in through the receive coil. The noise from the shift system has both a broad-band component, and discrete peaks that appear to be harmonics of the amplifier's 31 kHz switching frequency. One approach to the shift noise reduction can be an appropriate filtering of the shift amplifiers' outputs.

Fixing the shift noise problem would leave us dominated by the nuisance fluctuations generated from system instabilities. These are mainly related to modulations of empty-bore harmonics that arise from insufficiently filtered drive amplifier harmonics. The temporal instability of these deterministic empty-bore signals constitutes a drifting background that can not be removed from the detected data by a simple substraction [3]. In addition, fluctuations in the gain or the generation of harmonics by a SPION source contribute to the instability of the system. Since the variance in the empty-bore signals limits us 2× away from preamplifier noise floor, we expect an increase in SNR by another factor of 2 by the stabilization of the system. Approaches to alleviate system instability include changes on the shielding, groundings and the improvement of electrical contacts.

On preamplifier noise level, we are limited 6× away from coil noise dominance. The AD8429-based preamplifier used in the scanner setup has a voltage noise density of 1 $nV/\sqrt{Hz}$ and current noise density of 1.5 $pA/\sqrt{Hz}$. Previous work reports on improved low-noise amplifiers with a more than 2-fold lower input noise [6], leading to another factor of 2 in SNR improvement.

In its current state, the imager's detection limit (iron mass expected to yield an SNR = 1) was experimentally determined to be 150 ng of iron [1]. For frequencies between 30 kHz and 250 kHz, the receive signal S, in dBV for a 1 Am^2 sample is well approximated by $S = a\,f + b$ where f is in kHz, a = 0.08 and b = 84. Assuming we were able to reach preamplifier noise dominance, we expect a total factor of 10 in SNR improvement which equals a detection limit of 15 ng of iron (for Synomag COOH (micromod Partikeltechnologie GmbH, Rostock, Germany)).

V. Conclusion

Since unwanted interfering signals occur inevitably in every scanner setup, we believe that a precise characterization of any distorting signals is a mandatory first step towards MPI sensitivity enhancement. Knowing the sources of noise will help to effectively tailor future efforts to the improvement of the dominant contributors.

The noise and background signal characterization for our human-scale MPI scanner revealed that we are dominated by the noise generated from the shift amplifier and the system instability. These non-thermal noise sources limit us 10× or 60× away from the thermal noise level expected from the preamplifier and the coil resistance. Thus, future efforts will be dedicated to the mitigation of the shift noise and the stabilization of the system. Fixing these noise sources promises a total factor of 10 in SNR improvement which would lower our current detection limit to 15 ng of iron for the same scan time. Further improvements on the receive chain side (e.g. switching to a preamplifier with a lower input noise) are conceivable when striving for coil noise dominance.

Acknowledgments

Funding was provided by the National Institute of Biomedical Imaging and Bioengineering (NIBIB), of the National Institutes of Health (NIH) under award numbers 5T32EB1680, U01EB025121, and NSF GRFP 1122374.

Author's statement

Conflict of interest: Authors state no conflict of interest.

References

[1] E. Mattingly, Design, construction, and validation of magnetic particle imaging systems for rodent, primate, and human functional neuroimaging, PhD thesis, MIT, 2023,

[2] H. Paysen, O. Kosch, J. Wells, N. Loewa, and F. Wiekhorst. Characterization of noise and background signals in a magnetic particle imaging system. *Physics in Medicine & Biology*, 65(23):235031, 2020, doi:10.1088/1361-6560/abc364.

[3] K. Them, M. G. Kaul, C. Jung, M. Hofmann, T. Mummert, F. Werner, and T. Knopp. Sensitivity enhancement in magnetic particle imaging by background subtraction. *IEEE transactions on medical imaging*, 35(3):893–900, 2015, doi:10.1109/TMI.2015.2501462.

[4] T. Knopp, N. Gdaniec, R. Rehr, M. Gräser, and T. Gerkmann. Correction of linear system drifts in magnetic particle imaging. *Physics in Medicine & Biology*, 64(12):125013, 2019.

 © 2024 Infinite Science Publishing

[5] A. Barksdale, E. Mason, E. Mattingly, M. Sliwiak, J. Drago, and L. Wald. Shift coil assembly for a rotating permanent magnet ffl human-scale fmpi imager. *International Journal on Magnetic Particle Imaging IJMPI*, 8(1 Suppl 1), 2022, doi:10.18416/ijmpi.2022.2203067.

[6] M. Graeser, T. Knopp, P. Szwargulski, T. Friedrich, A. Von Gladiß, M. Kaul, K. M. Krishnan, H. Ittrich, G. Adam, and T. M. Buzug. Towards picogram detection of superparamagnetic iron-oxide particles using a gradiometric receive coil. *Scientific reports*, 7(1):6872, 2017, doi:10.1038/s41598-017-06992-5.

 © 2024 Infinite Science Publishing